ADVANCED FUNCTIONAL MATERIALS
www.afm-journal.de

Microstructures of YSZ and CGO Thin Films Deposited by Spray Pyrolysis: Influence of Processing Parameters on the Porosity

Barbara Scherrer, Julia Martynczuk, Henning Galinski, Jan G. Grolig, Selmar Binder, Anja Bieberle-Hütter, Jennifer L. M. Rupp, Michel Prestat, and Ludwig J. Gauckler*

Microstructures of yttria-stabilized zirconia (YSZ) thin films deposited by spray pyrolysis at 370 °C on sapphire are investigated. The as-deposited films are predominantly amorphous and crystallize upon heating at temperatures above 370 °C, developing grains in the range of 5 nm to several 100 nm. During post-deposition heat treatment up to 800 °C, ~ 50 vol% porosity develops in the center of the films with gradients towards almost dense interfaces to the air and substrate. The reason for this porosity is the decomposition of residues from the precursor and the free volume liberated due to crystallization. Dense YSZ thin films consisting of one monolayer of grains are obtained with annealing temperatures exceeding 1200 °C. In gadolinium-doped-ceria (CGO) thin films similar microstructures and porosity are found after low-temperature heat treatments indicating that the precursor residues due to the deposition method are the main cause of the porosity. Grain growth stagnation in annealed thin films is observed in both the YSZ and in CGO thin films. Stagnating grain growth in the thin films is rather caused by reduced grain boundary mobility, here predominately due to a "secondary phase", i.e., pores, than to other effects. The stagnation ceases at higher annealing temperatures after densification has taken place.

1. Introduction

Yttria-stabilized zirconia (YSZ) is a well known electrolyte material for solid oxide fuel cells (SOFC). In the last decade, research focuse on SOFCs operating at intermediate and low temperatures (<800 °C).[1–7] The lower operating temperatures require thinner electrolytes, e.g. in form of YSZ thin films to provide sufficient ionic conduction. Thin films of several hundred nanometers thickness can be deposited via (i.) vacuum techniques employing ceramic or metal-targets like in pulsed laser deposition (PLD) or sputtering and (ii.) deposition techniques based on liquid or gaseous organic-precursors, like chemical vapor deposition, atomic layer deposition, spin coating or spray pyrolysis.[8–14] For vacuum techniques, the thin films are deposited directly from solid targets resulting mostly in crystalline films; whereas for methods employing liquid or gaseous organic-precursors, the films are predominantly amorphous after deposition. YSZ thin films prepared with the latter are reported to develop porosity during post-deposition thermal treatments.[13,15–22] For example, YSZ thin films deposited by sol-gel routes show ~15 vol% porosity after annealing at 650 °C for 24 h, with pore sizes similar to those of the grains.[13,15] Pores were even observed in zirconia-based nanoparticles derived from metalorganic precursors.[23–26] Qualitative analysis by scanning or transmission electron microscopy and atom force microscopy of YSZ thin films prepared from metalorganic precursors revealed pore sizes in the range of 1 nm to 3.5 nm in films annealed at 600 °C.[13,15–19] Fully dense films were obtained only after annealing above 1200 °C. Zhu and Fan investigated the sintering behavior by dilatometry of nano-powders and characterized the densification process.[20] The highest densification rate was found at 950 °C. They claimed a full densification at 1000 °C, however, pores are still present at the surface of the specimen after 10 h, whereas Theunissen *et al.* report a full density at 1000 °C only after very long dwells (~100 h).[27] For sol–gel derived YSZ films, Dìaz-Parralejo et al. quantified the porosity indirectly by the refraction index.[21] Between 300 °C and 800 °C, the porosity ranged between 10 vol% and 30 vol%. Peters et al.[13] and Butz et al.[15] found a porosity of 15 vol% and 8 vol% by TEM for spin-coated sol-gel YSZ thin films annealed at 650 °C and 850 °C, respectively.

Typical precursor salts decompose in air at temperatures below 600 °C and below 800 °C in an inert atmosphere.[28–36] It is not surprising that remaining components from the organics were found within the as-deposited thin films, even though most of the solvents evaporate during deposition.[12,37,38] When analyzing fractured cross-sections of films deposited from organic precursors one might conclude that those films are dense.[39–46] However, as only fractured cross-sections or

---

B. Scherrer, J. Martynczuk, H. Galinski, J. G. Grolig, S. Binder, A. Bieberle-Hütter, J. L. M. Rupp, M. Prestat, L. J. Gauckler
Nonmetallic Inorganic Materials
ETH Zurich, Wolfgang-Pauli-Str.10,
CH-8093 Zurich, Switzerland
E-mail: barbara.scherrer@mat.ethz.ch

DOI: 10.1002/adfm.201200454

Table 1. Surface porosity and the corresponding processing parameters of YSZ thin films deposited by spray pyrolysis. The varied processing parameter in each section is printed bold.

	Surface porosity [%]	Spray rate [ml h^{-1}]	Spray time [min]	Annealing time [h]	Annealing temperature [°C]	Heating and cooling rate [°C min^{-1}]	Y	Zirconium salt	Solvent	Figure
Annealing conditions	11 ± 4	2.5	100	20	**800**	±3	8	St	St	5
	8 ± 1	2.5	100	20	**900**	±3	8	St	St	
	1.7 ± 0.4	2.5	100	20	**1000**	±3	8	St	St	
	0.11 ± 0.06	2.5	100	15	**1200**	±3	8	St	St	
	0	2.5	100	15	**1400**	±3	8	St	St	
	3.3 ± 0.5	2.5	100	**0**	1000	+3, −1000	8	St	St	
	1.3 ± 0.8	2.5	100	**5**	1000	+3, −1000	8	St	St	
	1.7 ± 0.4	2.5	100	**20**	1000	±3	8	St	St	
	1.2 ± 0.3	2.5	100	5	1000	±**1000**	8	St	St	
	1.3 ± 0.8	2.5	100	5	1000	+**3, −1000**	8	St	St	
	0.8 ± 0.3	2.5	100	20	1000	+**1000, −3**	8	St	St	
	1.7 ± 0.4	2.5	100	20	1000	±**3**	8	St	St	
Salt/Solvent	1.7 ± 1.1	5	50	20	1000	±3	8	**St**	**St**	6
	1.6 ± 0.8	5	50	20	1000	±3	8	**ZrO(NO$_3$)$_2$**	**St**	
	2.1 ± 0.7	5	50	20	1000	±3	8	**St**	**TEG:H$_2$O**	
	1.2 ± 0.7	5	50	20	1000	±3	8	**ZrO(NO$_3$)$_2$**	**TEG:H$_2$O**	
Depo. parameter	1.8 ± 0.6	**0.04**	100	20	1000	±3	8	St	St	
	1.7 ± 0.4	**2.5**	100	20	1000	±3	8	St	St	
	2.1 ± 0.5	**5**	100	20	1000	±3	8	St	St	
	1.7 ± 1.1	5	**50**	20	1000	±3	8	St	St	
	2.1 ± 0.5	5	**100**	20	1000	±3	8	St	St	
	0.3 ± 0.2	5	**10·(5’ + 20’ at 590 °C)**	20	1000	±3	8	St	St	7
Y content	1.5 ± 0.6	2.5	100	20	1000	±3	**0**	St	St	8
	0.8 ± 0.2	2.5	100	20	1000	±3	**3**	St	St	
	1.7 ± 0.4	2.5	100	20	1000	±3	**8**	St	St	
	0.9 ± 0.3	2.5	100	20	1000	±3	**10**	St	St	
	3.3 ± 0.8	2.5	100	20	1000	±3	**15**	St	St	

St denotes standard zirconium salt (zirconium acetate) and standard solvent composition (tetraethylene glycol (TEG) : polyethylene glycol 600: ethanol)

surfaces were analyzed by SEM some of the porosity might have been overlooked.

In this paper, the influence of the spray pyrolysis deposition parameters and post-process conditions on the densification and microstructures of YSZ thin films were investigated and the results are compared to those of CGO. Thereby, special emphasis was placed on analyzing the microstructure of the complete cross-section using focused ion beam (FIB) and scanning transmission electron microscopy (STEM).

2. Results and Discussion

After deposition, the YSZ thin films are mainly amorphous with a few nanometer-sized crystalline nuclei.[12] During annealing, the YSZ crystallizes and grain growth occurs. All YSZ thin films were crack-free after deposition as well as after annealing as proven with light microscopy and SEM. In this paper, the porosity, its origin, its three dimensional distribution and the effect of pores on the grain growth are studied to acquire knowledge on the microstructural evolution of YSZ thin films deposited by spray pyrolysis. Details of all thin film compositions and tested deposition and annealing conditions are summarized in **Table 1**.

2.1. Microstructural Evolution of Yttria-Stabilized Zirconia

In **Figure 1**, high-angle annular dark-field (HAADF) STEM micrographs of YSZ thin films are shown in the as-deposited state and after annealing at 600 °C and 1000 °C for 20 h each. In the HAADF STEM micrographs, the contrast is correlated

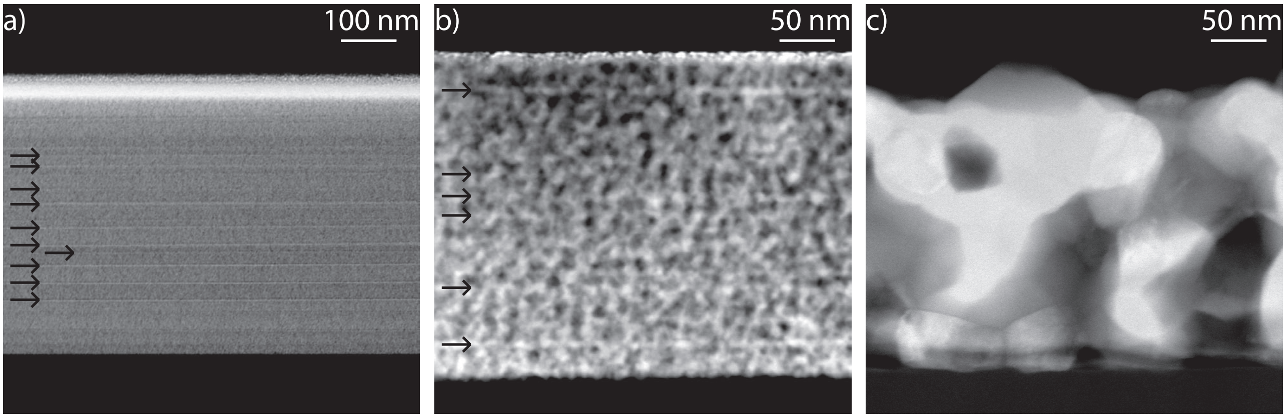

Figure 1. HAADF STEM micrographs showing the porosity in YSZ thin films annealed at different temperatures, a) as-deposited, b) annealed at 600 °C for 20 h, c) annealed at 1000 °C for 20 h. The arrows point towards the narrow brighter layers in a) and b) in the microstructures originating from the droplets' interfaces during deposition marking denser areas.

with the atomic number Z. This means that heavy elements or dense areas show up bright, and light elements or holes are darker. A non-uniform brightness was observed in the YSZ thin film after deposition (Figure 1a). The bright layers within the YSZ thin film (indicated by the arrows) are about 1 nm to 3 nm thick and up to 30 nm apart from each other. These thin layers (indicated by the arrows) correspond to the surface of the individual droplets forming the film upon deposition. One droplet in the dried state is about 30 nm thick. These layers are less pronounced in the films annealed at low temperature (Figure 1b). The YSZ also has a non-uniform brightness between the layers (Figure 1a). This gray shadowing originates from a variation of Z which could be caused either by the incorporated residues from the organic precursors or by pores. In atom probe measurements (not shown here), controlled evaporation was observed which leads to the conclusion that if there are pores, they are very small (<4 nm^3).[47] EDX mapping (not shown here) in STEM showed a lower concentration of zirconium and yttrium in the darker regions of the HAADF micrographs. No carbon variation and only a small oxygen depletion could be detected due to carbon contamination during scanning and their low x-ray interaction. Carbon and hydroxide were detected in x-ray photon spectroscopy (XPS) and their decomposition products by mass spectroscopy.[12] Therefore, we assume that the larger dark areas are most likely partly filled with amorphous carbon or zirconium hydroxide. After annealing at 600 °C for 20 h, the hydroxyl and carbon residuals have gasified resulting in pores (Figure 1b). The pores have a similar size as the grains of about 10 nm. After annealing at 1000 °C for 20 h, both the YSZ crystallites and the pores grew to about 110 nm, whereby the pores form a percolating network (Figure 1c).

2.2. Surface Versus Volume Porosity

A SEM micrograph of the surface, a FIB-cut cross-section and a fractured cross-section of an YSZ thin film deposited on sapphire and annealed at 800°C for 20 h are shown in **Figure 2**. Pores are clearly visible by SEM on the surface (Figure 2a) and within the FIB-cut cross-section (Figure 2b). In the fractured cross-section (Figure 2c), however, the dark areas are most likely also pores, but they cannot be distinguished from the grains that have been pulled out during fracturing of the sample and thus cannot conclusively be attributed to pores. For this reason, the porosity is in general difficult to detect in fractured cross-sections of thin films. Additionally, the contrast of the rough cross-section surface does not allow the evaluation of the porosity from the fractured cross-sections. Quantitative analysis of the porosity is only possible from SEM micrographs of the surface or FIB-cut cross-sections. The surface porosity was estimated to be about 11% and the cross-section porosity is about 43 vol%. The difference in porosity between the surfaces and the interiors of the films is not

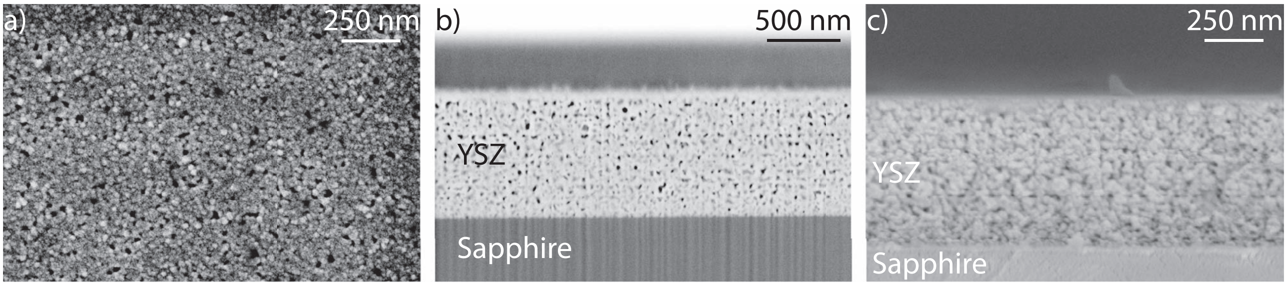

Figure 2. SEM micrographs of YSZ thin films deposited on sapphire and annealed at 800 °C for 20 h, a) top-view, b) FIB cross-section and c) fractured cross-section.

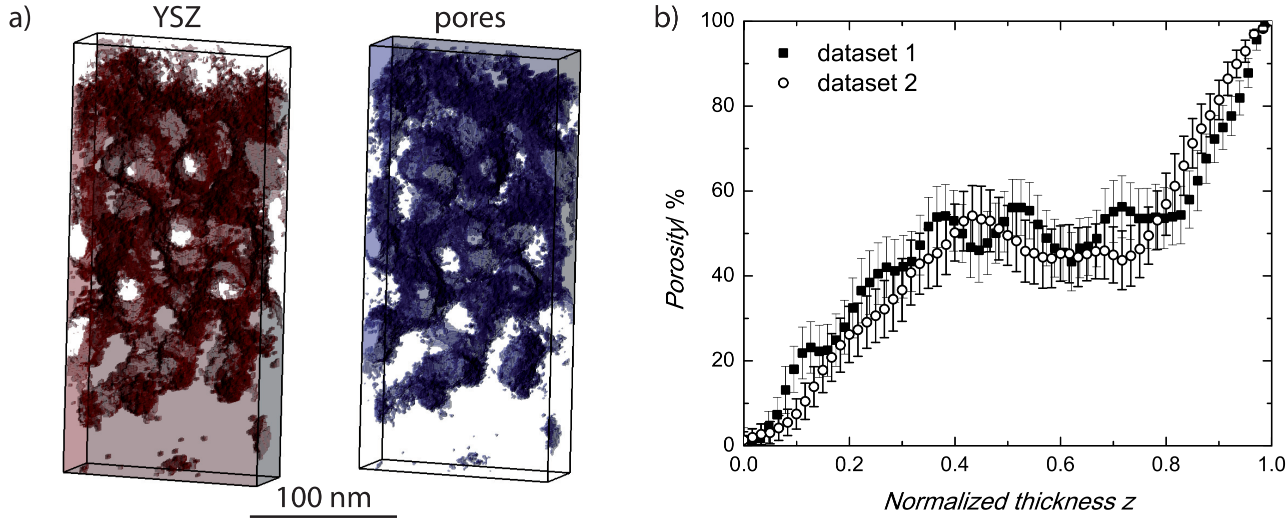

Figure 3. Porosity gradient within an YSZ thin film deposited on sapphire and annealed at 800 °C for 20 h, a) 3D reconstruction of YSZ (in brown, left side) and pores (in blue, right side) in the thin film, b) porosity gradient over the YSZ thin film cross-section from the thin film-substrate interface (z = 0) up to the surface of the thin film for two different samples. Please note that due to the roughness of the film the porosity approaches 100% at the film surface.

surprising, as it is known from conventional sintering studies that pores near the surface disappear faster, while pores in the volume of the film may undergo coarsening.[48] This is due to the smaller solid-solid boundary energy compared to the solid-vapor boundary energy which results in faster coarsening and densification of grains at the surface of the specimen.[49]

In **Figure 3**, 3D nano-tomography and the distribution of the porosity in YSZ thin films based on SEM micrographs of FIB cross-sections are shown. For clarity reasons only a small part of the reconstruction is depicted in Figure 3a. The YSZ is colored in brown, whereas the pores are shown in blue (Figure 3a). The selected image section is close to the interface between the substrate and thin film and ends on top of the thin film at its maximal thickness. The porosity is 0 vol% to 5 vol% at the interface to the substrate (z = 0), increases gradually (Figure 3b) to 50 ± 8 vol% inside the thin film (z = 0.5) and approaches 100% at the thin film's surface where the highest grain ends. Two different thin films annealed at 800 °C for 20 h were analyzed resulting in the two datasets. The porosity averaged over the whole film thickness is 43 vol%. The majority of the pores are connected to each other forming a 3D percolating network (Figure 3a). The surface porosity of the same annealing condition is 11% (Table 1).

It should be kept in mind that in FIB-cut cross-sections the analysis of the porosity is possible but becomes difficult for pore sizes smaller than 5 nm. In these cases, TEM tomography would be necessary. We assume that in the thin film annealed at 800 °C for 20 h the pores are larger than 5 nm, since we found that the pores are of the same size as the grains (see section 2.1). The surface and interface porosity is about 5 to 10 times smaller than the bulk porosity.

2.3. Origin of the Porosity

DSC/TG measurements were performed in static air in order to analyze the amount of remaining volatile species within the spray pyrolyzed YSZ directly after deposition and during annealing. In **Figure 4**, the enthalpy evolution and mass loss are

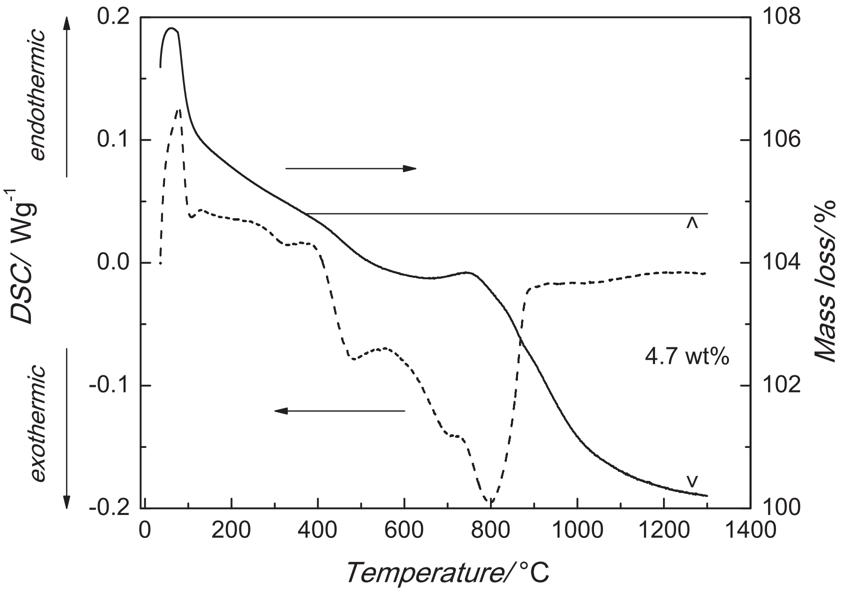

Figure 4. Mass loss and enthalpy evolution of as-deposited YSZ measured in static air.

shown. A detailed discussion of the enthalpy evolution is published in Ref.[12] Below the deposition temperature of 370 °C, a mass loss of 3 wt% was found, which is due to the liberation of adsorbed water and carbon dioxide as evidenced by mass spectroscopy elsewhere.[12] The total mass loss between 370 °C and 1300 °C of 4.7 ± 0.1 wt% is due to the loss of water and CO_2 as decomposition products. This corresponds to a volume fraction between 19 ± 8 vol% (100% water from zirconium hydroxide) and 14 ± 8 vol% (100% CO_2 from amorphous carbon). The volume fraction was calculated taking the theoretical density of YSZ of 6.01 g cm^{-3} and the one of $Zr(OH)_4$ and amorphous carbon of 3.25 g cm^{-3} and 1.8 g cm^{-3}, respectively. The evolving porosity of the film annealed at 800 °C for 20 h is 43 ± 12 vol% evidenced by FIB-cut cross-sections. In addition to these 43 vol% of porosity in the annealed film, a volume loss (16 ± 13 vol% of the as-deposited state) due to one-dimensional shrinkage in z direction of the film occurred during annealing. This results in a total volume change from the as-deposited to the annealed state of 52 ± 22 vol%. Assuming that the volatile species also evaporate during annealing at 800 °C for 20 h, it is possible to correlate this total volume change (52 ± 22 vol%) with the resulting volume due to the mass loss up to 1300 °C (between 19 ± 8 vol% and 14 ± 8 vol%) and the free volume change of 3 vol% to 5 vol% during crystallization. The remaining part of 28 vol% to 35 vol% is assigned to porosity within the as-deposited thin film. This leads to the conclusion that the variation in the brightness in the HAADF STEM micrographs (Figure 1a) of the as-deposited thin films might be attributed to both pores and uncompleted oxidation of precursor residuals. In accordance to pores in the as-deposited films, also mesoporosity of 1 nm to 7 nm in diameter was found inside powder grains by others following a similar fabrication route.[23–26,50]

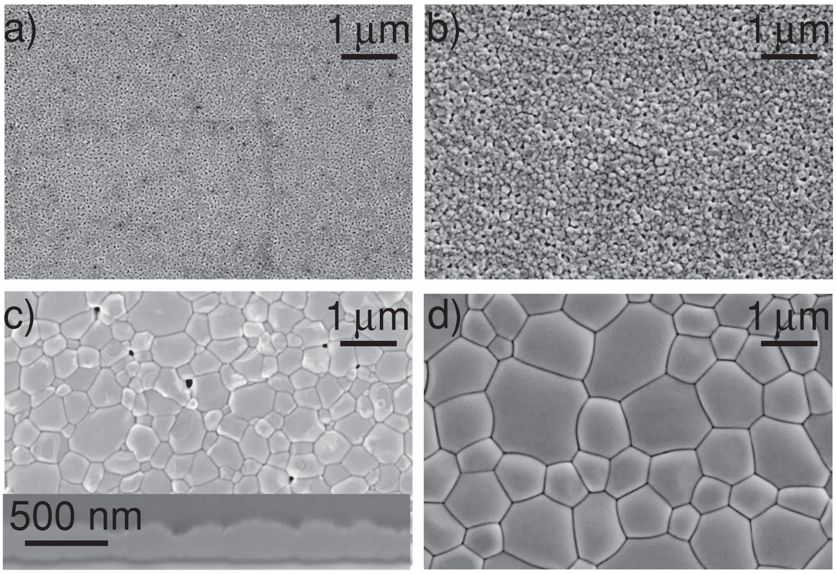

Figure 5. SEM micrographs of YSZ thin films annealed under different conditions in top-view; a) 800 °C for 20 h (average grain size: 17 ± 5 nm), b) 1000 °C for 20 h (average grain size: 110 ± 50 nm), c) 1200 °C for 15 h (average grain size: 680 ± 50 nm), FIB cross-section inserted at the bottom and d) 1400 °C for 15 h (average grain size: 1400 ± 700 nm).

2.4. Processing Parameters and Their Influence on the Microstructural Evolution of Spray Pyrolyzed YSZ Thin Films

In Table 1, the surface porosity of the YSZ thin films and all the tested deposition and annealing conditions are summarized. Here, the surface porosity was used to get an idea of the influence of the tested conditions on the porosity, assuming that if surface porosity occurs, cross-section porosity is even more pronounced. Additionally, the annealing conditions were chosen in order to obtain microstructures with a grain and pore size which is easily resolved by SEM.

2.4.1. Annealing Conditions

In **Figure 5**, SEM top-view micrographs of YSZ thin films after isothermal annealing in the temperature range from 800 °C to 1400 °C are shown. See Figure 2a for a micrograph with higher magnification of the specimen annealed at 800 °C. The average grain size increases with increasing annealing temperature from around 17 ± 5 nm after 800 °C for 20 h to 1400 ± 700 nm at 1400 °C for 15 h. The film thicknesses are between 200 nm and 700 nm. For annealing temperatures above 1200 °C, the grain size grew to the size of the film thickness and therefore the films consist of one monolayer of YSZ grains only (see Figure 5c, inset). Grain boundary grooving started at the thin film surface and interface to the substrate. Upon annealing, the surface porosity decreases from 11% to fully dense films above 1200 °C (Table 1). These findings also agree well with those in other pore-free wet-processed yttria-doped zirconia thin films and powders, which were obtained at annealing temperatures above 1200 °C.[15,16,19,21,51–53] Theunissen et al., report a full density at 1000 °C only after very long dwells (~100 h).[27] Zhu and Fan claimed a full densification after a short dwell of only 10 h.[20] However at the surface of their SEM micrograph, pores are visible.

Therefore, the development of surface porosity during isothermal annealing was investigated. A slightly higher surface porosity of 3.3% was found for the annealing at 1000 °C without an isothermal dwell. This is not surprising as these samples had no time to densify at elevated temperature. The heating and cooling rates of the annealing at 1000 °C were varied. Rapid heating and slow cooling halves the surface porosity meaning that a high burn-off rate of the residuals influences positively the surface porosity. However, the porosity cannot be prevented by a fast heating.

2.4.2. Precursor and Deposition Parameters

As described in section 2.3, the remaining carbon is one origin of the porosity. Therefore, the salt and solvent precursors were varied in order to study their influence on the

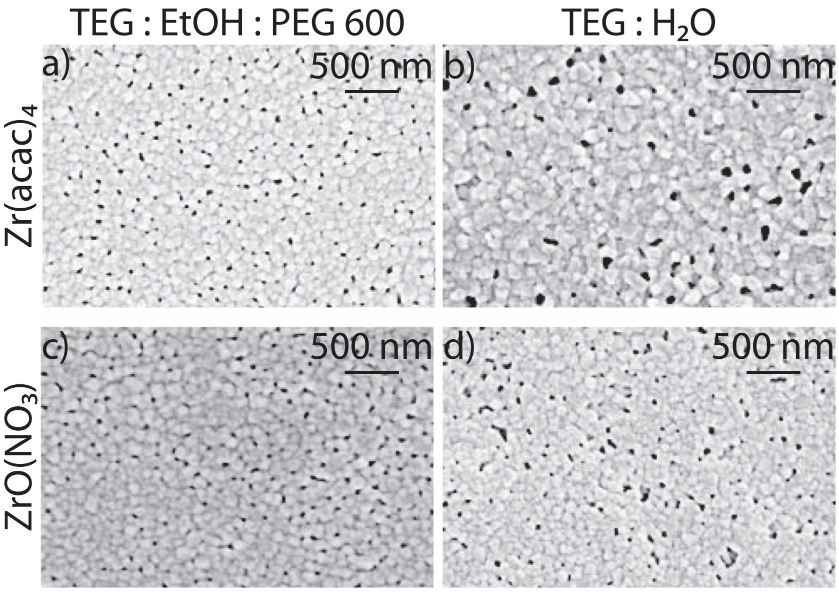

Figure 6. Top-view SEM micrographs showing surface porosity of YSZ thin films deposited from different zirconium salts and solvents and annealed at 1000 °C for 20h, top-view.

porosity. Zirconium acetylacetonate or zirconyl nitrate as salts in tetraethylene glycol-polyethylene glycol 600-ethanol and tetraethylene glycol-water solution were tested. In **Figure 6**, the top-view micrographs are shown. The microstructure as well as the surface porosities did not change significantly for all four precursors. In addition, the solution feeding rate of the precursor solution was varied from 0.04 ml h^{-1} to 5 ml h^{-1}. The effect on the surface porosity (1.8% to 2.1%) was also negligible.

Intermittent spraying with curing steps at 590 °C was investigated, as curing might facilitate the evaporation of residues from the precursors. After 5 min of spraying at 370 °C, the spray cone was interrupted and the substrate was heated to 590 °C for 20 min. This sequence was repeated five times and the thin film was subsequently annealed at 1000 °C for 20 h. This intermitted spraying resulted in a significant decrease of surface porosity to only 0.3% (**Figure 7**a). Nevertheless, porosity is still present within the YSZ thin film as illustrated in the corresponding cross-section micrograph (Figure 7b).

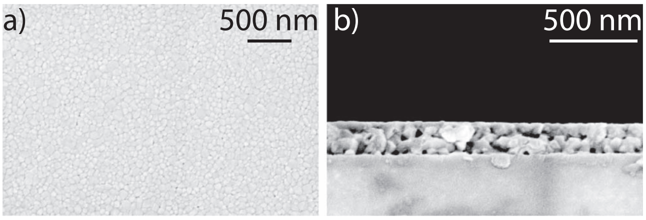

Figure 7. SEM micrographs of intermitted sprayed YSZ thin films annealed at 1000 °C for 20 h, a) dense top-view and b) porous fractured cross-section.

2.4.3. Yttria Content

Yttria is known to be moisture sensitive[54] and could therefore lead to porosity due to the observed hydroxide. The yttria content was varied between 0 mol% and 15 mol% with respect to the deposited oxide. The top-view SEM micrographs are shown in **Figure 8**. No significant influence on the surface porosity was found (Table 1). To the best of our knowledge, no information on the influence of the yttria content on the amount of porosity is available in literature. In contrast to the surface porosity, the average grain size changes with the yttria content. For the pure zirconia thin films as well as the 3 mol% and 8 mol% YSZ films, the average grain size is about 95 nm which is 25% smaller than that of the films with higher yttrium content (Figure 8). The differences in grain size are most likely due to the so-called solute drag effect caused by the different yttrium contents.

2.5. Comparison of the Microstructural Evolution of Yttria-Stabilized Zirconia (YSZ) and Gadolinium-Doped Ceria (CGO) Thin Films

In **Figure 9** HAADF STEM micrographs of CGO thin films deposited on sapphire are shown. In the case of the CGO annealed at 600 °C, the grain and pore sizes are in a similar range as in the YSZ films (cf. (Figure 1b and (9a). Until now however, pores in spray-pyrolyzed CGO are only mentioned by Bieberle-Hütter et al., whereas others report dense microstructures.[39,55–57] This is most likely due to the insufficient resolution of SEM and/or the difference in porosity at the thin film's surface and its interior as discussed in section 2.2. Therefore, it is utmost important to analyze the microstructures down to the nanometer scale. Just a few remaining pores at the thin film–substrate interface are visible for the CGO specimen annealed at 1000 °C (Figure 9b). Additionally, some pores with a size of about 5 nm which are incorporated in CGO grains are present (indicated by arrows). The small pores incorporated inside the CGO grains indicate that in CGO the grain boundaries are no longer pinned to pores at 1000 °C. CGO films annealed at 1000°C have smaller and fewer pores than the YSZ films (cf. (Figure 1c) and (9b)). Also the grain boundaries of YSZ are less mobile and thus cannot separate from the pore. As the melting point of CeO_2 is about 300 K lower than the one of zirconia and since the diffusivity is proportional (in K) to the melting point, the densification of CGO is faster.[58,59] This results in the lower porosity found for the CGO films.

2.6. Grain Growth of YSZ Thin Films

The grain size evolution of YSZ thin films deposited on sapphire for different annealing temperatures is shown in

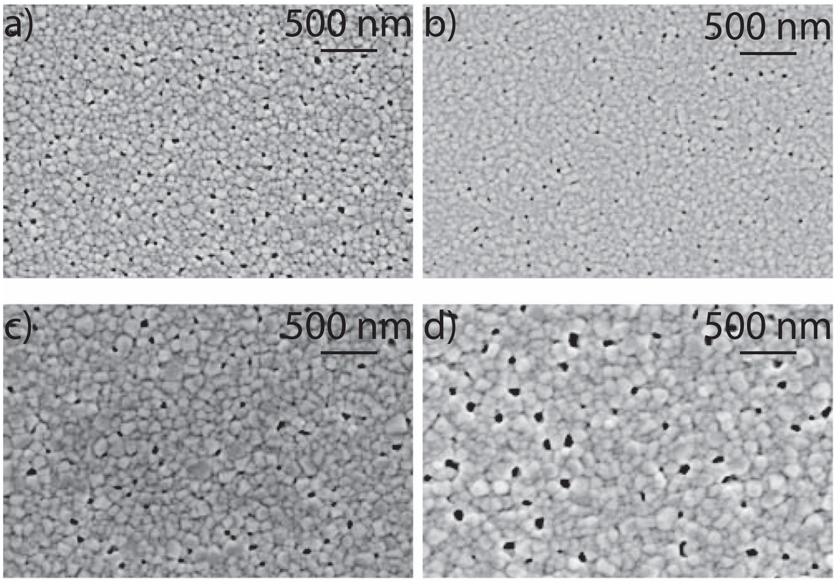

Figure 8. SEM micrographs show surface porosity of yttria-doped zirconia thin films annealed at 1000 °C for 20 h with respect to their yttria content, a) 0 mol% (ZrO_2; average grain size: 90 ± 40 nm), b) 3 mol% (average grain size: 100 ± 50 nm), c) 10 mol% (average grain size: 120 ± 50 nm) and d) 15 mol% yttria-doped zirconia (average grain size: 140 ± 60 nm).

Figure 10. After one to two hours of annealing at temperatures below 1000 °C, the grain growth stagnates at different grain sizes. Gorman and Anderson reported also such a grain growth stagnation at the similar grain sizes for unsupported and therefore unstrained, but porous YSZ thin films deposited by spin-coating.[17] Above 900 °C, normal grain growth was reported for YSZ thin films made by spin-coating and precipitated powders.[27,60] A similar grain growth stagnation is reported in literature for other ceramics than YSZ like CGO as well as metal thin films.[39,61,62] Several effects are known to cause such a stagnation or inhibition of the grain growth, e.g. secondary phases, solute drag, strain, grain size to film thickness ratio, or triple junctions.[63–66] If the grain size is comparable to the film thickness, grain boundary grooving occurs and leads to grain growth stagnation as well.[63,67] This latter process can be excluded in the temperature range below 1000 °C for the investigated YSZ films as the grain size is always about three times smaller than the film thickness. Shvindlerman and Gottstein investigated the efficiency of different drag mechanism due to impurities, vacancies, particles and triple junctions for stagnating grain growth in metals.[64] As they highlighted, triple junction drag can be even more effective than particle drag for reducing the mobility of grain boundaries. However, at least for yttria it has been shown that the triple junction drag is not significant compared to pore drag at low temperatures.[68] Yan *et al.* pointed out that the grain boundaries pinned by secondary phases like pores and particles are less mobile than those pinned by solute drag[66] and Li *et al.* discussed that the influence of solute drag is more pronounced on the stagnation of grain growth than the influence of microstrain.[69] We therefore conclude that particles and pores, among the effects discussed above, have the most pronounced influence on the grain boundary mobility in these thin ceramic ZrO_2 and CeO_2-based film. This is also supported by Chen, who postulates that the often observed deviation from the parabolic grain growth is due to an underestimated high porosity in the investigated specimens.[65] Marder et al. observed in nanocrystalline yttria a parabolic grain growth for porosities smaller than 3%, whereas for higher porosities the grain growth is decelerated.[68] This is in accordance with the very fast grain growth kinetics found in dense YSZ thin films deposited by PLD which were also amorphous after deposition.[10]

In essence, it can be concluded that in the case of spray pyrolyzed YSZ and CGO thin films, the stagnation of grain growth at annealing temperatures below 1000 °C is caused by reduced grain boundary mobility due to a "secondary phase", i.e. pores in this case, rather than by other effects.

3. Summary and Conclusion

The development of porosity and the grain growth in YSZ thin films deposited by spray pyrolysis are investigated upon annealing. In the as-deposited thin films about 28 vol% to 35 vol% porosity is present with pore sizes smaller than 4 nm. During annealing, additional porosity develops within the YSZ thin films which is due to the decomposition and outgassing of residues in the films originating from the precursor salts and solvents used in the spray pyrolysis process. After annealing at 800 °C, the porosity of the YSZ film inside the cross-section is with ~43 vol% much higher than the porosity found at the film surface and at the interface to the substrate.

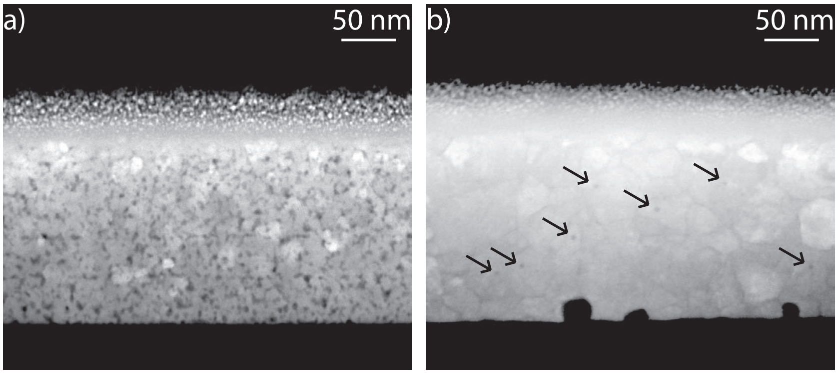

Figure 9. HAADF STEM micrographs showing porosity in CGO thin films on sapphire annealed a) at 600 °C for 10 h and b) at 1000 °C for 10 h. The arrows indicate small dark regions.

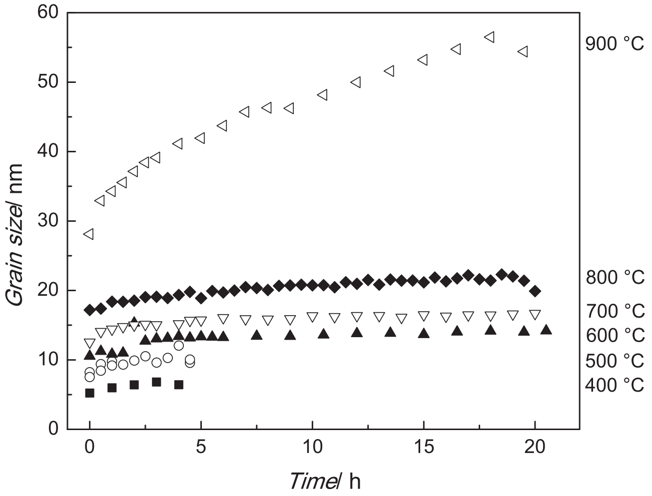

Figure 10. Grain size evolution at different temperatures for YSZ thin films deposited on sapphire.

For an annealing temperature of 1000 °C, the porosity at the YSZ thin film surface ranges from 0.8% to 3.3% and is independent on the deposition parameters such as the precursor, spray time and solution feed rate. Also, the yttria content as well as the heating and cooling rate of the annealing procedure do not result in a different surface porosity.

Annealing temperatures above 1200 °C result in dense YSZ thin films; however, these films consist of a monolayer of YSZ grains. The observed porosity is due to the deposition technique and is not specific for YSZ, as we also found pores in CGO thin films deposited by spray pyrolysis. However, the onset temperature of the densification process depends on the mobility of the ions and thus is material specific.

Grain growth stagnation is observed in YSZ films upon annealing. We suggest that the pores found within the spray pyrolyzed YSZ thin film contribute significantly to the reduction of the grain boundary mobility leading to the reported stagnating grain growth during isothermal annealing.

We conclude from this study that fully dense YSZ or CGO thin films deposited by precursor-based methods like spray pyrolysis are hardly possible, especially if the thin films are annealed at low temperatures (<1000 °C). The porosity prevents the use of these methods for fabricating an electrolyte layer for application in a micro-SOFC where a dense layer is required for separating the oxidizing and reducing atmospheres. However, for electrode materials and insulators in electrochemical redox-cycling experiments such a mesoporosity is highly recommended.

4. Experimental Section

Deposition: YSZ thin films were deposited by air-blast spray pyrolysis. Details about this method can be found in previous work.[70,71] The precursor solution was pumped to a spray gun (Compact 2000KM, Bölhoff Verfahrenstechnik, Germany) where it was atomized with 1 bar air pressure and sprayed on a substrate heated to 370 ± 5 °C. Random orientated sapphire (Stettler, Switzerland) was used as substrates. The precursor solution consisted of zirconium acetylacetonate (Alfa Aesar, 99% purity) or zirconyl nitrate (Fluka, 99% purity) and yttrium chloride hydrate (Alfa Aesar, 99.9% purity) dissolved in two different solutions: the standard solutions consisted of 80 vol% tetraethylene glycol (TEG, Aldrich, 99% purity), 10 vol% polyethylene glycol 600 (PEG 600, Fluka) and 10 vol% ethanol (Fluka, 99.9% purity) and alternatively a solution made of 90 vol% TEG and 10 vol% deionized water was used. The total salt concentration was 0.05 mol l^{-1}. A molar ratio of Zr: Y = 85.2: 14.8 was chosen to obtain a 8 mol% yttria-stabilized zirconia ($Zr_{0.852}Y_{0.148}O_{2-\delta}$) composition.[72] For film deposition, the liquid flow rate was varied between 2.5 ml h^{-1} and 5 ml h^{-1} and the spray time between 50 min and 100 min as listed in Table 1. In parallel, YSZ powder was sprayed with a liquid flow rate of 50 ml h^{-1} for 10 h keeping all other parameters constant.

For comparison, CGO ($Ce_{0.8}Gd_{0.2}O_{2-\delta}$) thin films were deposited using the same setup with slightly adjusted deposition parameters: the substrate temperature was set to 390 ± 5 °C, the deposition time to 105 min and the solution flow rate to 5 ml h^{-1}. The CGO precursor solution consisted of 0.08 mol l^{-1} cerium nitrate (Alfa Aesar, 99.5% purity) and 0.02 mol l^{-1} gadolinium chloride (Alfa Aesar, 99.9% purity) dissolved in 90 vol% tetraethylene glycol (TEG, Aldrich, 99% purity) and 10 vol% deionized water.

Microstructure: Top-view microstructures of the thin films were characterized by a field-emission-gun scanning-electron-microscopy (FEG-SEM, Zeiss LEO Gemini 1530, Germany) with an in-lens detector. Prior to imaging, the thin films were coated with platinum in order to avoid charging and to enable imaging at higher magnification. The cross-sectional views were prepared by focused ion beam technique (FIB, Carl Zeiss, CrossBeam NVision 40, Germany) with a gallium liquid metal ion source and a gas injection system. After electron beam deposition of carbon in SEM mode at low scan speeds, the thin films were protected by a carbon cap and trenches were milled from 13 nA down to 10 pA at 30 kV. The evaluation of the surface and volume porosity was analyzed via ImageJ (version 1.36b) to determine the area fractions of black and white images.[73] The micrographs were captured at randomly selected locations. For each sample, at least six SEM micrographs were used to evaluate the porosity. In the error propagation calculation, systematic errors resulting from uncertainties of the thickness, porosity, mass change and density were taken into account. Stacks of multiple cross-sections were aligned recursively by Stackreg[74] and reconstructed using AVS Express (Advanced Visual Systems Inc.). The voxel-size of the resulting tomographic micrographs is $0.5 \times 0.5 \times 4.0$ nm^3. Transmission-electron-microscope lamellae were cut free with trenches from both sides with 13 nA and 3 nA at 30 kV. After the lift-out was performed with a micromanipulator (Kleindiek, MM3M, Germany), the lamellae were polished to ion transparency with currents as low as 10 pA at 30 kV. Finally, the amorphization of the specimens due to the Ga-ion cutting were kept at minimum by low-kV showering them for several seconds at 5 kV and 2 kV. Scanning transmission electron microscopy (STEM) in high-angle annular dark-field (HAADF) mode was used to characterize YSZ and CGO thin films on sapphire which were prepared by spray pyrolysis and annealed at 600–1000 °C for 10–20 h. The microscope was a FEI Tecnai F-30 (field emission gun) with an accelerating voltage of 300 kV.

The phase and average grain sizes were analyzed with X-ray diffraction (XRD, PANalytical X'pert, Netherlands) equipped with a copper radiation source operated at 45 kV and 40 mA with parallel beam geometry. The average grain sizes were determined from the (111) peak width using the Scherrer equation.[75] The instrumental broadening was corrected with an unstrained sintered YSZ pellet from powder with micrometer-sized grains. For grain sizes larger than 80 nm, the intercept lengths of grain sizes from SEM micrographs were measured using Lince 2.4.2β software.[76] More than 300 grains were averaged. The average film thickness was determined from at least 10 measurements by using a surface profilometer (Alpha Step 500, KLA Tencor).

The heat evolution of as-deposited spray pyrolysis YSZ was measured by differential-scanning-calorimetry combined with thermogravimetry (DSC/TG, Netzsch STA 449C, calibrated with the standard from Netzsch 6.223.5-91.2). As-deposited amorphous YSZ was scratched off the sapphire substrate and the obtained powder was measured in a Pt crucible up to 1300 °C at 3 °C min^{-1}. Buoyancy and heat flow corrections were performed with the data from a second run using fully crystallized YSZ spray-pyrolyzed powder of the same mass.

Acknowledgements

The authors thank Anna Evans, Ashley S. Harvey, Lorenz Holzer, Meike Schlupp and Joakim Reuteler for stimulating discussions, and Eva Sediva for some of the SEM image analyses. The authors acknowledge support by the Electron Microscopy of ETH Zurich (EMEZ). Financial support by the following Swiss institutions is gratefully acknowledged: the Swiss National Science Foundation (SNF) within the framework of the Sinergia project ONEBAT (CRSI22-126830), the Competence Centre Energy and Mobility (CCEM) within the framework of the ONEBAT project, the Competence Centre for Materials Science and Technology (CCMX) within the framework of the NANCER project, Swiss Electric Research (SER) within the framework of the ONEBAT project as well as the Korean-Swiss Science and Technology Cooperation.

Received: February 13, 2012
Revised: March 21, 2012

[1] B.-K. Lai, K. Kerman, S. Ramanathan, *J. Power Sources* **2011**, *196*, 1826.
[2] A. Evans, A. Bieberle-Hütter, J. L. M. Rupp, L. J. Gauckler, *J. Power Sources* **2009**, *194*, 119.
[3] U. P. Muecke, D. Beckel, A. Bernard, A. Bieberle-Hütter, S. Graf, A. Infortuna, P. Müller, J. L. M. Rupp, J. Schneider, L. J. Gauckler, *Adv. Funct. Mater.* **2008**, *18*, 3158.
[4] K. Kerman, B.-K. Lai, S. Ramanathan, *J. Power Sources* **2011**, *196*, 2608.
[5] H. Huang, M. Nakamura, P. C. Su, R. Fasching, Y. Saito, F. B. Prinz, *J. Electrochem. Soc.* **2007**, *154*, B20.
[6] I. Garbayo, A. Tarancón, J. Santiso, F. Peiró, E. Alarcón-Lladó, A. Cavallaro, I. Gràcia, C. Cané, N. Sabaté, *Solid State Ionics* **2010**, *181*, 322.
[7] S. Rey-Mermet, Y. Yan, C. Sandu, G. Deng, P. Muralt, *Thin Solid Films* **2010**, *518*, 4743.
[8] S. Heiroth, T. Lippert, A. Wokaun, M. Dobeli, J. L. M. Rupp, B. Scherrer, L. J. Gauckler, *J. Eur. Ceram. Soc.* **2010**, *30*, 489.
[9] H. Huang, J. H. Shim, C. C. Chao, R. Pornprasertsuk, M. Sugawara, T. M. Gur, F. B. Prinz, *J. Electrochem. Soc.* **2009**, *156*, B392.
[10] S. Heiroth, R. Frison, J. L. M. Rupp, T. Lippert, E. J. Barthazy Meier, E. Müller Gubler, M. Döbeli, K. Conder, A. Wokaun, L. J. Gauckler, *Solid State Ionics* **2011**, *191*, 12.
[11] N. I. Karageorgakis, A. Heel, A. Bieberle-Hütter, J. L. M. Rupp, T. Graule, L. J. Gauckler, *J. Power Sources* **2010**, *195*, 8152.
[12] B. Scherrer, S. Heiroth, R. Hafner, J. Martynczuk, A. Bieberle-Hütter, J. L. M. Rupp, L. J. Gauckler, *Adv. Funct. Mater.* **2011**, *21*, 3967.
[13] C. Peters, A. Weber, B. Butz, D. Gerthsen, E. Ivers-Tiffée, *J. Am. Ceram. Soc.* **2009**, *92*, 2017.
[14] R. Frison, S. Heiroth, J. L. M. Rupp, K. Conder, E. Müller, M. Horisberger, M. Döbeli, L. J. Gauckler, **2012**, Unpublished.
[15] B. Butz, H. Störmer, D. Gerthsen, M. Bockmeyer, R. Krüger, E. Ivers-Tiffée, M. Luysberg, *J. Am. Ceram. Soc.* **2008**, *91*, 2281.
[16] K. A. Erk, C. Deschaseaux, R. W. Trice, *J. Am. Ceram. Soc.* **2006**, *89*, 1673.
[17] B. P. Gorman, H. U. Anderson, *J. Am. Ceram. Soc.* **2002**, *85*, 981.
[18] C. Sakurai, T. Fukui, M. Okuyama, *J. Am. Ceram. Soc.* **1993**, *76*, 1061.
[19] K. T. Miller, F. F. Lange, D. B. Marshall, *Journal of Materials Research* **1990**, *5*, 151.
[20] Q. Zhu, B. Fan, *Solid State Ionics* **2005**, *176*, 889.
[21] A. Díaz-Parralejo, R. Caruso, A. L. Ortiz, F. Guiberteau, *Thin Solid Films* **2004**, *458*, 92.
[22] F. F. Lange, *Science* **1996**, *273*, 903.
[23] M. R. Alvarez, M. J. Torralvo, *Colloids and Surfaces A: Physicochemical and Engineering Aspects* **1996**, *113*, 165.
[24] V. Raju, S. Jaenicke, G.-K. Chuah, *Applied Catalysis B: Environmental* **2009**, *91*, 92.
[25] M. Rezaei, S. M. Alavi, S. Sahebdelfar, Z.-F. Yan, *Powder Technology* **2006**, *168*, 59.
[26] I. M. Hung, K.-Z. Fung, D.-T. Hung, M.-H. Hon, *Journal of the European Ceramic Society* **2008**, *28*, 1161.
[27] G. S. A. M. Theunissen, A. J. A. Winnubst, A. J. Burggraaf, *Journal of the European Ceramic Society* **1993**, *11*, 315.
[28] B. A. A. Balboul, *Journal of Analytical and Applied Pyrolysis* **2010**, *88*, 192.
[29] G. A. M. Hussein, B. A. A. Balboul, *Powder Technology* **1999**, *103*, 156.
[30] H. M. Ismail, *Powder Technology* **1995**, *85*, 253.
[31] H. M. Ismail, *Journal of Analytical and Applied Pyrolysis* **1991**, *21*, 315.
[32] H. B. Wang, C. R. Xia, G. Y. Meng, D. K. Peng, *Materials Letters* **2000**, *44*, 23.
[33] H. Song, Y. Jiang, C. Xia, G. Meng, D. Peng, *Journal of Crystal Growth* **2003**, *250*, 423.
[34] H. Z. Song, H. B. Wang, J. Zhang, D. K. Peng, G. Y. Meng, *Materials Research Bulletin* **2002**, *37*, 1487.
[35] O. Stryckmans, T. Segato, P. H. Duvigneaud, *Thin Solid Films* **1996**, *283*, 17.
[36] J. Madarász, S. Kaneko, M. Okuya, G. Pokol, *Thermochimica Acta* **2009**, *489*, 37.
[37] P. Peshev, I. Stambolova, S. Vassilev, P. Stefanov, V. Blaskov, K. Starbova, N. Starbov, *Materials Science and Engineering B* **2003**, *97*, 106.
[38] R. López, R. Romero, F. Martín, J. R. Ramos-Barrado, D. Leinen, *Surface and Interface Analysis* **2006**, *38*, 277.
[39] J. L. M. Rupp, A. Infortuna, L. J. Gauckler, *Acta Materialia* **2006**, *54*, 1721.
[40] J. L. M. Rupp, C. Solenthaler, P. Gasser, U. P. Muecke, L. J. Gauckler, *Acta Materialia* **2007**, *55*, 3505.
[41] I. Kosacki, T. Suzuki, V. Petrovsky, H. U. Anderson, *Solid State Ionics* **2000**, *136–137*, 1225.
[42] T. Suzuki, I. Kosacki, H. U. Anderson, *Solid State Ionics* **2002**, *151*, 111.
[43] T. Suzuki, I. Kosacki, H. U. Anderson, *J. Am. Ceram. Soc.* **2002**, *85*, 1492.
[44] I. Kosacki, V. Petrovsky, H. U. Anderson, *Appl. Phys. Lett.* **1999**, *74*, 341.
[45] C. C. Chen, H. U. Anderson, M. M. Nasrallah, *U.S. Padent No. 5,494,700 Patent*, **1996**.
[46] N. I. Karageorgakis, A. Heel, T. Graule, L. J. Gauckler, *Solid State Ionics* **2011**, *192*, 464.
[47] C. Oberdorfer, G. Schmitz, *Microsc. Microanal.* **2011**, *17*, 15.
[48] R. M. German, *Crit. Rev. Solid State Mater. Sci.* **2010**, *35*, 263.
[49] M. N. Rahaman, *Ceramic processing and sintering*, CRC Press/Taylor and Francis Group, Boca Raton **2003**.
[50] B. Ksapabutr, E. Gulari, S. Wongkasemjit, *Mater. Chem. Phys.* **2004**, *83*, 34.
[51] D. Yang, H. Conrad, *Scripta Mater.* **2010**, *63*, 328.
[52] C. Sakurai, T. Fukui, M. Okuyama, *ChemInform* **1993**, *24* DOI: 10.1002/chin.199327035.
[53] K. T. Miller, C. J. Chan, M. G. Cain, F. F. Lange, *J. Mater. Res.* **1993**, *8*, 169.
[54] M. Winterer, R. Nitsche, H. Hahn, *Nanostruct. Mater.* **1997**, *9*, 397.

[55] A. Bieberle-Hütter, P. Reinhard, J. L. M. Rupp, L. J. Gauckler, *J. Power Sources* **2011**, *196*, 6070.
[56] K. Konstantinov, I. Stambolova, P. Peshev, B. Darriet, S. Vassilev, *Int. J. Inorg. Mater.* **2000**, *2*, 277.
[57] J. L. M. Rupp, L. J. Gauckler, *Solid State Ionics* **2006**, *177*, 2513.
[58] H. G. Scott, *J. Mater. Sci.* **1975**, *10*, 1527.
[59] P. Patnaik, *Handbook of Inorganic Chemicals*, McGraw-Hill, **2003**.
[60] J. Dong, M. Z. Hu, E. A. Payzant, T. R. Armstrong, P. F. Becher, *J. Nanosci. Nanotechnol.* **2002**, *2*, 161.
[61] H. Natter, M. S. Loffler, C. E. Krill, R. Hempelmann, *Scr. Mater.* **2001**, *44*, 2321.
[62] A. Michels, C. E. Krill, H. Ehrhardt, R. Birringer, D. T. Wu, *Acta Mater.* **1999**, *47*, 2143.
[63] Z. An, H. Ding, Q. Meng, Y. Rong, *Scr. Mater.* **2009**, *61*, 1012.
[64] L. S. Shvindlerman, G. Gottstein, *Zeitschrift fur Metallkunde* **2004**, *95*, 239.
[65] I. W. Chen, *Interface Sci.* **2000**, *8*, 147.
[66] M. F. Yan, R. M. Cannon, H. K. Bowen, in *Ceramic Microstructures '76*, (Eds: R. M. Fulrath, J. A. Pask), Westview Press, Boulder, Colorado **1976**, 276.
[67] H. J. Frost, C. V. Thompson, D. T. Walton, *Acta Metall. Mater.* **1990**, *38*, 1455.
[68] R. Marder, R. Chaim, C. Estournès, *Mater. Sci. Eng.: A* **2010**, *527*, 1577.
[69] J. Li, J. Wang, G. Yang, *Scr. Mater.* **2009**, *60*, 945.
[70] O. Wilhelm, S. E. Pratsinis, D. Perednis, L. J. Gauckler, *Thin Solid Films* **2005**, *479*, 121.
[71] D. Perednis, O. Wilhelm, S. E. Pratsinis, L. J. Gauckler, *Thin Solid Films* **2005**, *474*, 84.
[72] B. Scherrer, A. Rossi, J. Martynczuk, M. D. Rossell, A. Bieberle-Hütter, J. L. M. Rupp, R. Erni, L. J. Gauckler, *J. Power Sources* **2011**, *196*, 7372.
[73] W. S. Rasband, *U. S. National Institutes of Health*, Bethesda, Maryland, USA, **1997–2011**, http://imagej.nih.gov/ij/.
[74] P. Thevenaz, U. E. Ruttimann, M. Unser, *Image Processing, IEEE Transactions on* **1998**, *7*, 27.
[75] P. Scherrer, *Nachrichten von der Königlichen Gesellschaft der Wissenschaft zu Göttingen: Mathematisch-physikalische Klasse* **1918**, 98.
[76] S. L. D. Lucato, Darmstadt University of Technology, Darmstadt, Germany- **1998**.